DOI: 10.1002/ejic.200700083

Localization and Delocalization of Spin Density in Mixed-Valence (V^{IV}/V^{V}) $[(V_2O_3)_2(PhPO_3)_4\subset F]^{-n}$ (n = 1, 2): Theoretical and Experimental Studies

Nguyen Huu Thong,[a] Jabor K. Jabor,[a] Reinhard Stößer,[a] Manfred Meisel,*[a] and Burkhard Ziemer[a]

Keywords: Adsorption / DFT calculation / ESR / Hyperfine structure / Vanadium / Cage compounds

Based on XRD and optimized structures of the cage compound $[(V_2O_3)_2(PhPO_3)_4\subset F]^{-n}$ in singlet (n = 1) and doublet (n = 2) states DFT calculations were carried out to determine the energies and spin density distribution for the symmetries D_{2d}, C_{2v} and C_s. It turned out, that the cage with C_s symmetry not only represents the energetically more stable doublet system (with respect to D_{2d} and C_{2v}-symmetries) but also corresponds to the real compound under study. The SOMO of the S = 1/2 cage represents an antibonding state and the volume of the cage in this state is larger than that in the S = 0 state. The calculated ESR hyperfine coupling constants are in acceptable agreement with those determined by ESR. Experimentally the localization/delocalization of spin density was determined via ESR as a function of temperature and adsorption of the cage on Al_2O_3, respectively. A proposal is given for the localization/delocalization of spin density based on thermally driven changes of the cage symmetry in combination with the hopping of the unpaired electron inside the cage.

Introduction

Vanadium organophosphonates (VOP) represent a large group of organic-inorganic hybrid materials. They have gained increasing research interest not only due to their structural diversity and interesting redox properties but also due to potential applications in different areas, for example catalysis[1] and intercalation.[2] The anions $[(V_2O_3)_2(RPO_3)_4\subset F]^{-n}$ as mentioned in the title of the paper own cage structures and represent interesting model system for (i) spectroscopic and (ii) quantum-chemical investigations.

As a part of our research, we are interested in preparation and study of vanadium organophosphonate cages in the presence of anionic templates. In the past few years several cage structures were prepared in the presence of halide anions, e.g. F^-,[3–5] Cl^-,[6–8] and Br^-.[9] Up to now some questions are still not fully answered: the function of the template anion, the electronic structures including the localization/delocalization of spin density in the cages, the reversibility of the redox reactions and the potential application fields.

In principle, the one-electron reduction of the vanadium cage $[(V_2O_3)_2(RPO_3)_4\subset F]^{-1}$ (R = organic group) should result in the formation of paramagnetic species in a doublet state (S = 1/2). Hardly anything is known about the extent of spin density distribution over the cage. Quantum-chemical calculation and ESR investigation at different temperature in fluid and solid matrices should provide answers to open questions. The unpaired electron in the cage structure can be localized at a single vanadium nucleus or delocalized over 2, 3 or 4 vanadium nuclei. ESR is a powerful tool to detect and monitor such kinds of paramagnetic species. A simple delocalization model will be used to elucidate the phenomena which are observed by ESR. The quantum-chemical calculations (DFT method) start with structures of forced symmetries of the cage covering D_{2d}, C_{2v} and C_s and end up with experimentally determined structures (XRD). For comparison the structurally related system $VO(acac)_2$ was investigated by both methods.

The cage compound $[(V_2O_3)_2(PhPO_3)_4\subset F]^{-n}$ in singlet and doublet states represents a suitable model not only for the study of localization/delocalization phenomena of the spin density but also for the reversibility of redox reactions.

It should be mentioned at this point, that the investigation preselected in this paper concerns chemical compounds in different states of aggregation. The quantum-chemical over the gaseous phase, the ESR over the liquid and the XRD the solid phase. But we would like to show that even in the case of the cage compounds, the cage properties will change under the influence of internal and external limiting factors. The cage itself based on its spherical structure is able to preserve most of these unique properties. Therefore, it seems to be justified to perform the investigation as outlined in this paper.

[a] Institut für Chemie, Humboldt-Universität zu Berlin, Brook-Taylor-Str. 2, 12489 Berlin, Germany
Fax: +49-30-2093-7468
E-mail: manfred.meisel@chemie.hu-berlin.de

Results and Discussion

Calculation Method

The hybrid version of the DFT method with the B3LYP-functional[10] in connection with the basis set 6-311G* of triple zeta quality for V, O and F and with the basis set 4-21G for the organic structure of the cage has been used.[11] All the calculations have been carried out with the quantum chemical code GAUSSIAN 03.[12]

Three types of structures were calculated: (i) The *simplified structures* of forced symmetry and a replacement of the organic rests by H atoms to save computer time, (ii) the *complete structures* like the simplified structures with the real organic rests and (iii) the so-called *"X-ray" structure* using structural parameters obtained from XRD measurements.

The calculations here refer to the cage anions only; the influence of the cations will not be taken into account.

Simplified Structures with D_{2d} Symmetry

The structures of both the anions $[(V_2O_3)_2(PhPO_3)_4{\subset}F]^{-n}$ in singlet (n = 1) and doublet state (n = 2) have been totally optimized. As displayed in parts a and b of Figure 1 the optimized geometry of the cage in the singlet state leads to an integer network with an F^- anion in the centre of the cage. In contrast, for simplification the doublet structure may be thought to be composed from several fragments: two times V_2O_3, four times HPO_3 and one F^-.

Remarkable is the total delocalization of the additional electron in the doublet structure. Each V atom has the same spin density of 0.39 (the sum of the spin densities is greater than 1 because of the negative spin densities at some O atoms, see Table 5). The comparison between some geometry parameters of the anion cages in the singlet and the doublet state is shown in Table 1. Going from the singlet state to the doublet state both the terminal V–O and the bridging V–O bonds are almost unchanged while the V–OP and V–F distances become larger. That means, an additional electron, delocalized in the cage, causes a larger volume of the cage. This effect can be explained by the analysis of the SOMO of the doublet structure (Figure 2). All V–OP bonds in that orbital own antibonding character, and the occupation of that orbital weakens the bonds between the V atoms in V_2O_3 fragments and the O atoms of the HPO_3 fragments with the consequence of enlarging the cage. The larger V–F distance in the doublet structure is therefore caused by the enlarging of the cage based on the antibonding character of the bond between the V atoms and the O atoms of HPO_3 fragments and not by a weaker bond between the V and F atoms.

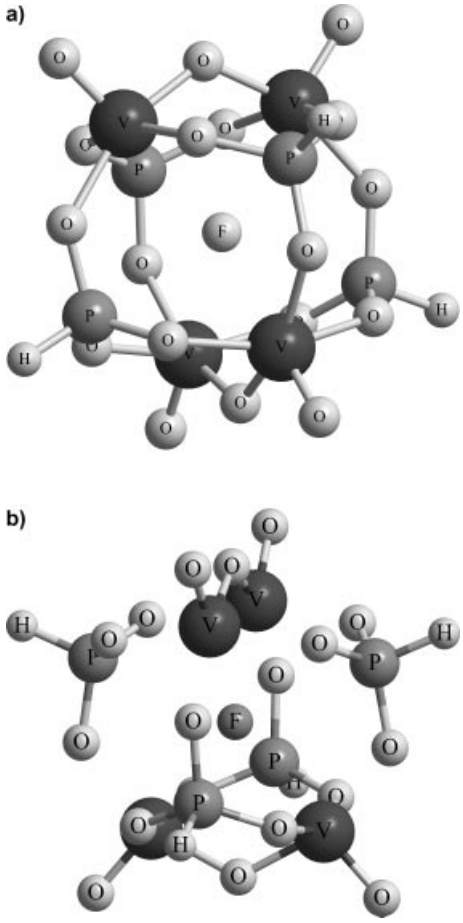

Figure 1. a) Calculated structure of the cage in the D_{2d} singlet state. b) Calculated structure of the cage in the D_{2d} doublet state.

Table 1. Comparison of some geometry parameters of the cage anions with D_{2d} symmetry in the singlet and doublet structure.[a]

Structural element	Distance [pm] Singlet	Doublet
V–O(brdg)	179.1	179.0
V–O(term)	155.8	157.0
V–O(–P on plane)	195.1	197.0
V–O(–P out of plane)	194.3	198.0
V–F	249.0	250.4
Energy (au)	–6599.540075	–6599.547719

[a] brdg = bridging; term = terminal; on plane = the bonds on the same plane as the V_2O_3 fragment; out of plane = the bonds out of plane which contains the V_2O_3 fragment; au = atomic unit = 627.51 kcal/mol.

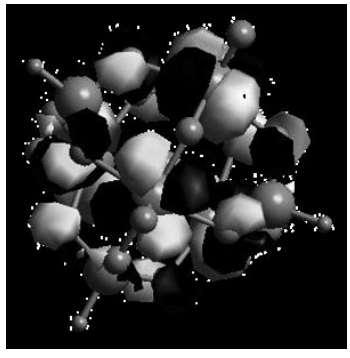

Figure 2. SOMO of the D_{2d} doublet.

The delocalization of the unpaired electron in this model structure follows directly from the symmetry assumed. Under energetic aspects the doublet structure is a bit more stable than the singlet one (see Table 1).

Simplified Structures with C_{2v} Symmetry

The structures of both the anions $[(V_2O_3)_2(PhPO_3)_4\subset F]^{-n}$ in singlet (n = 1) and doublet state (n = 2) have been totally optimized. The optimized geometry of the cage in the singlet state leads to an integer network with an F^- anion in the centre of the cage similar to the singlet structure in the D_{2d} symmetry (Figure 1, a). While the doublet structure can be regarded as a composite of one V_2O_3 fragment, one F^- anion in the centre of the cage and the residue of the cage (Figure 3). The unpaired electron is localized in the V_2O_3 fragment with equal spin densities of 0.7 for each of the two V atoms (see Table 5). Each V atom should have the oxidation number of 4.5 in this fragment. As in the case discussed above, the V^{IV}–OP and V^{IV}–F^- distances are larger than the V^V–OP and V^V–F distances in the corresponding singlet structure (see Table 2). It should be noted that the V^V–F distances in the doublet structure are even smaller than V^V–F distances in the singlet structure of the same symmetry (241.0 compared with 247.0 pm). Assuming C_{2v} symmetry, the doublet structure is more stable than the singlet one.

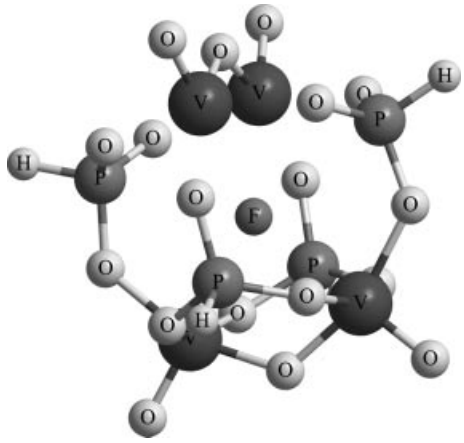

Figure 3. Calculated structure of the cage in the C_{2v} doublet.

Table 2. Comparison of some geometry parameters of the cage anions with C_{2v} symmetry in the singlet and doublet structure.[a]

Structural element	Distance [pm] Singlet	Doublet
V^V–O(brdg)	179.0	179.0
V^{IV}–O(brdg)		178.9
V^V–O(term)	155.0	156.0
V^{IV}–O(term)		157.0
V^V–O(–P on plane)	195.0	193.0
V^{IV}–O(–P on plane)		202.0
V^V–O(–P out of plane)	194.0	195.0
V^{IV}–O(–P out of plane)		200.0
V^V–F	247.0–249.0	241.0
V^{IV}–F		260.0
Energy (au)	–6599.540075	–6599.552346

[a] brdg = bridging; term = terminal; on plane = the bonds on the same plane as the V_2O_3 fragment; out of plane = the bonds out of plane which contains the V_2O_3 fragment; au = atomic unit = 627.51 kcal/mol.

Structures of C_s Symmetry

Simplified Structures with C_s Symmetry

The structures of both the anions $[(V_2O_3)_2(PhPO_3)_4\subset F]^{-n}$ with singlet (n = 1) and doublet (n = 2) states have been totally optimized. The optimized geometry of the cage in the singlet state leads to an integer network with an F^- anion in the centre of the cage similar to the singlet structure in the D_{2d} symmetry (Figure 1, a) while the doublet structure formal can be regarded as a composite of one V_2O_3 fragment, one F^- anion in the centre of the cage and the residue of the cage (Figure 4). The unpaired electron appears to be localized on the V_2O_3 fragment which is positioned in the plane of symmetry. The consequence is, that the two V atoms are no more equivalent: two values for the spin density result: 1.07 and 0.10 (Figure 5, a). That means, the unpaired electron is more or less localized at one V atom with enlarged V^{IV}–F distance. The other V atom can be regarded as a "quasi V^V " ion. It stands out, that the V^{IV}–O(brdg) and V^{IV}–OP distances are enlarged, but the terminal bonds V^{IV}–O(term) remain nearly unchanged (see Table 3). Furthermore, the distances of the V^V–O(brdg) in the symmetry plane is remarkable shortened (169.0 pm). The SOMO is in general of antibonding character. But there is a bonding pi-character of the bond between the V^V atom and the bridging O atom in the C_s plane (Figure 5, b). Under energetic aspects the doublet structure here also appears to be more stable than the singlet one.

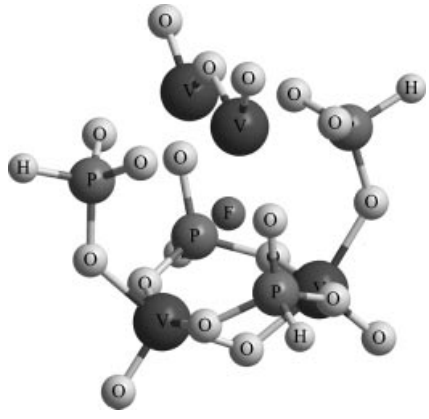

Figure 4. Calculated structure of the cage in the C_s doublet state.

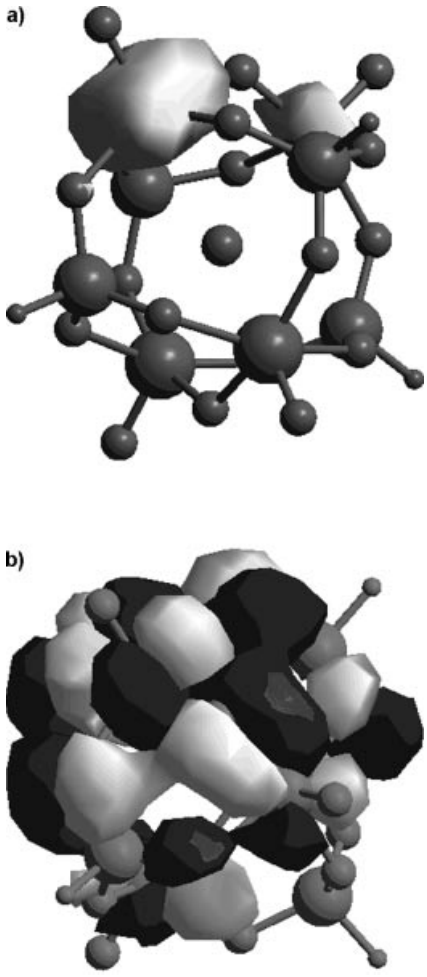

Figure 5. a) Spin density of the doublet state with C_s symmetry b) SOMO of the C_s doublet state.

Table 3. Comparison of some geometry parameters of the cage anions with C_s symmetry in the singlet and doublet structure.

Structural element	Distance [pm] Singlet	Doublet
V^{IV}–O(brdg)[a]	179.0	193.0
V^{V}–O(brdg)[a]	179.0	169.0
V^{V}–O(brdg)[b]	179.0	179.0
V^{IV}–O(term)[a]	155.0	157.0
V^{V}–O(term)[a]	155.0	157.0
V^{V}–O(term)[b]	155.0	156.0
V^{IV}–O(–P on plane)[a]	195.0	202.0
V^{V}–O(–P on plane)[a]	195.0	203.0
V^{V}–O(–P on plane)[b]	195.0	193.0
V^{IV}–O(–P out of plane)[a]	194.0	202.0
V^{V}–O(–P out of plane)[a]	194.0	197.0
V^{V}–O(–P out of plane)[b]	194.0	194.0
V^{IV}–F[a]	246.0	260.0
V^{V}–F[a]	248.0	261.0
V^{V}–F[b]	250.0	241.0
Energy (au)	–6599.540069	–6599.556154

[a] On the C_s-plane. [b] Perpendicular to the C_s-plane. brdg = bridging; term = terminal; on plane = the bonds on the same plane as the V_2O_3 fragment; out of plane = the bonds out of plane which contains the V_2O_3 fragment; au = atomic unit = 627.51 kcal/mol.

The Complete and X-ray Doublet Structures with C_s Symmetry

The cages in the complete doublet structure with C_s symmetry and the so-called X-ray doublet structure have been calculated. This has been done in order to find out what kind of influences can be expected by the organic rests of the cage. As the results of the calculation show, there is no essential influence of the phenyl substituents on the localization of the unpaired electron or on the geometry of the cage (column 2 and 3 of Table 4). The optimized parameters of the complete structure are in a good agreement with those of the XRD experiments. The calculated C_s symmetry of the cage anion is compatible with that in the crystal (for related compounds see ref.[3]). But one has to note, that the spin localization at one V atom in the X-ray structure is not so strong as in the gaseous phase and that the V–F distances in the symmetry plane, determined by XRD, are remarkable shorter and more asymmetric than those in the complete structure calculated for the gaseous phase (Table 4). The most probable reason for this finding should be the packing effect in the solid state, which results in deformation of the cages and the fragments V_2O_3 and HPO_3 come closer together (see also the ESR spectra from solutions of the cage with $S = 1/2$).

Table 4. Comparison of some geometry parameters of the simplified, the complete and the X-ray doublet structures with C_s symmetry.

Structural element	Distance [pm] Simplified	Complete	X-ray
V^{IV}–O(brdg)[a]	193.0	193.0	186.0
V^{V}–O(brdg)[a]	169.0	169.0	171.0
V^{V}–O(brdg)[b]	179.0	180.0	181.0
V^{IV}–O(term)[a]	157.0	158.0	157.0
V^{V}–O(term)[a]	157.0	158.0	159.0
V^{V}–O(term)[b]	156.0	157.0	157.0
V^{IV}–O(–P on plane)[a]	202.0	201.0	197.0
V^{V}–O(–P on plane)[a]	203.0	201.0	202.0
V^{V}–O(–P on plane)[b]	193.0	191.0	189.0
V^{IV}–O(–P out of plane)[a]	202.0	201.0	202.0
V^{V}–O(–P out of plane)[a]	197.0	197.0	197.0
V^{V}–O(–P out of plane)[b]	194.0	193.0	192.0
V^{IV}–F[a]	260.0	268.0	240.3
V^{V}–F[a]	261.0	267.0	250.4
V^{V}–F[b]	241.0	241.0	243.4

[a] On the C_s-plane. [b] Perpendicular to the C_s-plane. brdg = bridging; term = terminal; on plane = the bonds on the same plane as the V_2O_3 fragment; out of plane = the bonds out of plane which contains the V_2O_3 fragment; au = atomic unit = 627.51 kcal/mol.

Comparison of the Simplified Doublet Structures Having Different Symmetries

Table 5 shows the energies, the spin densities and the Fermi contact coupling constants of the simplified doublet structures in regarded symmetries. A B3LYP calculation of $VO(acac)_2$ (acac = acetylacetonate) in C_2 symmetry has also been carried out for comparison (the last line of Table 5). First there is a tendency of delocalization of the additional electron in the higher symmetries. Second, the cage anion

seems energetically to prefer the less symmetric geometry C_s. Third, the Fermi contact coupling constants depend strongly of the forced symmetries. Fourth, both the spin densities and the Fermi contact coupling constants of the cage in C_s symmetry and $VO(acac)_2$ in C_2 are very similar. This fact reflects the similar electronic structure of the VO groups and the similar {4+1} coordination of the V atoms in both.

Table 5. Comparison of the energies, the spin densities and the Fermi contact coupling constants between simplified doublet structures with different symmetries.

Symmetry/ energy [au]	Spin density on the V atoms	Extent of localization	Fermi contact couplings [Gauss]
D_{2d}	0.39; 0.39	fully	–27.54931
–6599.547719	0.39; 0.39	delocalized	
C_{2v}	0.02; 0.02	localized on	–1.64340
–6599.552346	0.69; 0.69	one V_2O_3 fragment	–50.50854
C_s	1.07; 0.10	almost	–85.28022
–6599.556154	0.01; 0.01	localized on	–7.76268
		one V atom	–0.72122
			–0.72122
$C_2/VO(acac)_2$	1.12 on V	almost localized	–85.78522
–1710.053571	–0.13 on O	on the V atom	

The Experimental Findings of ESR Spectroscopy

As mentioned above, from theoretical and experimental point of view it was of interest to have a simple model system to compare the obtained results for the cage structure with those of the model. For structural reasons $VO(acac)_2$ was selected because this system has several advantages. It is well known for a long time, it bears a similar structural unit (VO_5), and in dilute solutions there is no doubt that only one ^{51}V centre is present in the molecular unit with $S = 1/2$.[13,14] The corresponding experimental and simulated ESR spectra are collected in Figure 6 and Figure 7, respectively. The spectra displayed in Figure 6 represent the resonances of V^{IV} species in fluid (Figure 6, a and c) and frozen (Figure 6, b and d) solutions. The shape of the spectra in the fluid solution is characterized by an incomplete averaging out of the anisotropic hyperfine splitting by molecular motion (tumbling). It means, beside higher order hyperfine effects the typical dependence of the line width of the individual hyperfine-lines on the nuclear spin quantum number m_I results.[15] The spectra could be reproduced by simulation taking into account the line width effects mentioned above together with third order effects of hyperfine splitting (Figure 7). Note that the different patterns of the spectra (Figure 6, a and c) are caused by the different viscosity and polarity of the solvents used and are manifested in the pa-

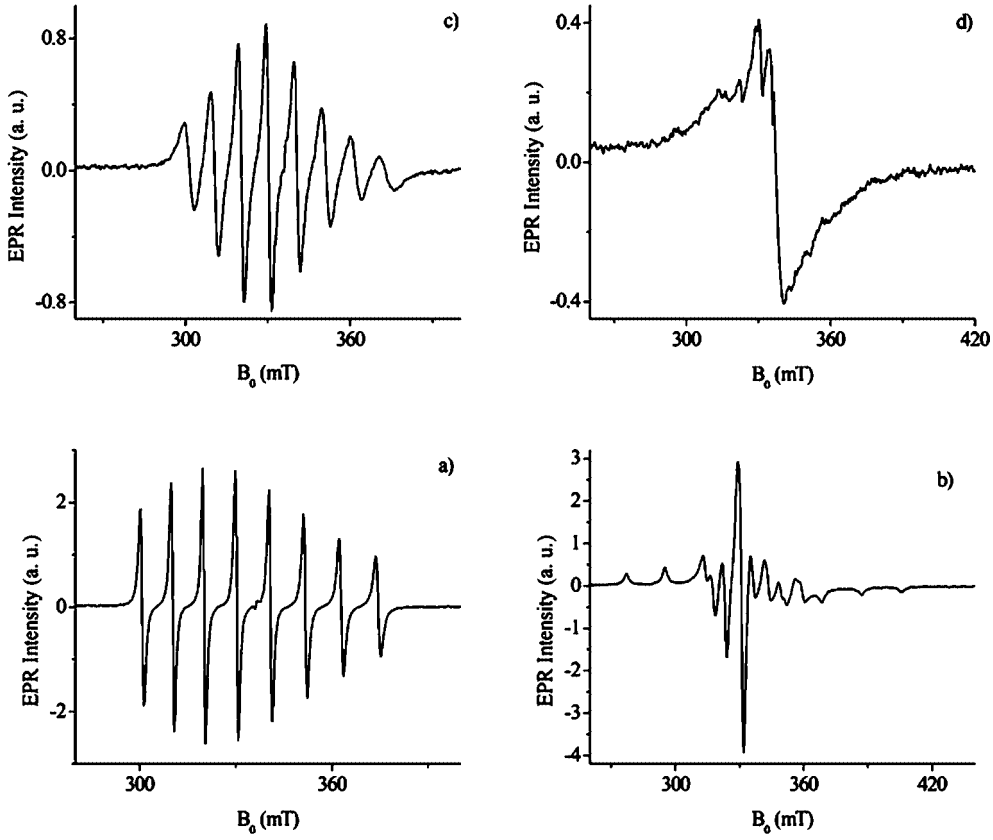

Figure 6. ESR spectra of $VO(acac)_2$, a) CH_3CN solution at 293 K, b) CH_3CN solution at 77 K; c) DMSO solution at 293 K; d) DMSO solution at 77 K.

rameters {α, β, and γ} of the simulation[16] (see caption of Figure 7). The result of the quantum-mechanical calculations of this model system is already given in Table 5.

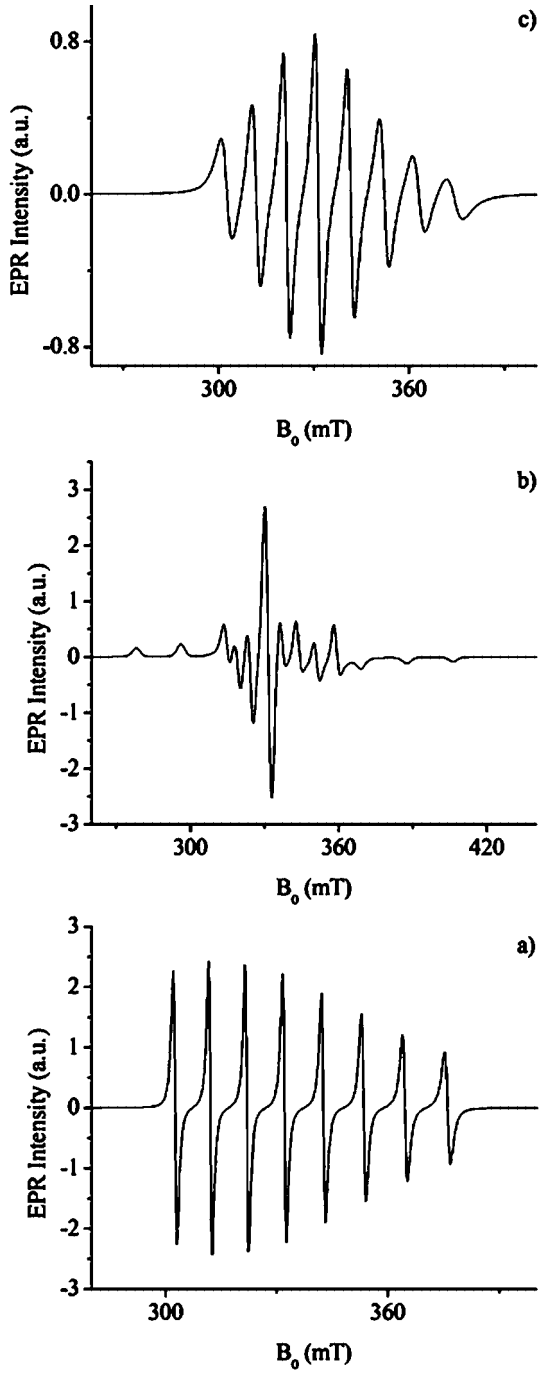

Figure 7. Simulated ESR spectra of $VO(acac)_2$, a) CH_3CN solution at 293 K (g_{iso} = 1.971, A_{iso} = 105 G, α = 10.31, β = –0.79, γ = 0.19); b) CH_3CN solution at 77 K ($g_{\|}$ = 1.956, $A_{\|}$ = 183.5 G, $g_{\perp}$ = 1.986, $A_{\perp}$ = 62.5 G); c) DMSO solution at 293 K (g_{iso} = 1.969, A_{iso} = 102.3 G, α = 21.60, β = –2.76, γ = 2.0).

The reduction of $[Ph_3PCH_2CH_3][(V_2O_3)_2(PhPO_3)_4 \subset F]$ with I^- in CH_3CN at room temperature results in the formation of paramagnetic species in a doublet state (S = 1/2). The ESR spectrum of the paramagnetic species (Figure 8, a) exhibits an isotropic 29-line pattern with g_{iso} = 1.964 and A_{iso} = 28.6 G, due to the symmetrical interaction of the unpaired electron with 4 vanadium nuclei in the cage.[4,5,17,18] Generally, the spin density can be delocalized homogeneously, if the cage is surrounded by a symmetrical solvation shell. The consequence of that is the observation of equal values of the hyperfine coupling constant for the four vanadium nuclei (^{51}V, I = 7/2) in the cage. A further condition for this observation is a fast reorientation of the cage ($\tau_R \approx 10$ ns) which averages out a possible residue of anisotropy of the hyperfine patterns. Under these conditions one can observe a 29 line spectrum. So, any process which will change the tumbling rate of the cage and/or make it asymmetrical should be responsible for to the change of the ESR spectra. One way to do so is to measure the ESR spectra at lower temperature. The ESR spectrum of frozen CH_3CN solution (77 K) exhibits an 8 line pattern (Figure 8, b) which reflects also a large portion of anisotropic interactions. These effects are manifested in the known dependency of the intensity on the nuclear spin quantum number m_I.[15] It is noteworthy that the spectral change between fluid and frozen solutions is reversible.

Another way to make the cage asymmetrical is to adsorb it on the surface of e.g. alumina. The symmetry of the cage should be changed due to specific interactions between the cage and the active sites of the Al_2O_3 with a tendency to localize of the unpaired electron at one or two vanadium atoms assisted by the geometrical shape of the cage. The scale of these specific interactions[13,14] is of essential influence on the localization/delocalization of the spin density of the doublet state. The ESR spectrum (Figure 8, c) of Al_2O_3 after contact with the paramagnetic CH_3CN solution shows an axial anisotropic eight-line spectrum inclusive some degree of broadening due to coupling of the unpaired electron to a single ^{51}V nucleus (I = 7/2). The spectrum represents in its essential feature the envelope of adsorbed and aggregated cages. Broadening of the ESR signals may be attributed to the presence of a spin-spin exchange between the aggregated paramagnetic species in the solid. Lowering the temperature to 77 K yields the spectrum as displayed in Figure 8 (d).

Removing the aggregated species from the system by washing with CH_3CN results in a nearly complete anisotropic 8-line spectrum (Figure 8, e) with an axial feature, $g_{\|}$ = 1.935, $A_{\|}$ = 195 G, $g_{\perp}$ = 1.986 and $A\perp$ = 72 G (compare also with the spectra displayed in Figure 6). In this case the spin density must be "fully" localized at one ^{51}V-nucleus in the cage. Obviously, the immobilization of the cages at the surface of Al_2O_3 is sufficiently strong. It is evidenced by the ESR spectrum taken at 77 K (Figure 8, f) which gave no essential differences with respect to that obtained at 293 K. Furthermore these facts not only confirm the process of adsorption[13,14,19] of the cage but also the adsorption-induced localization of spin density in the cage. The solution of the cage (S = 1/2) coexisting with the {adsorbence/adsorbate} yield, when separately measured at 293 K, a

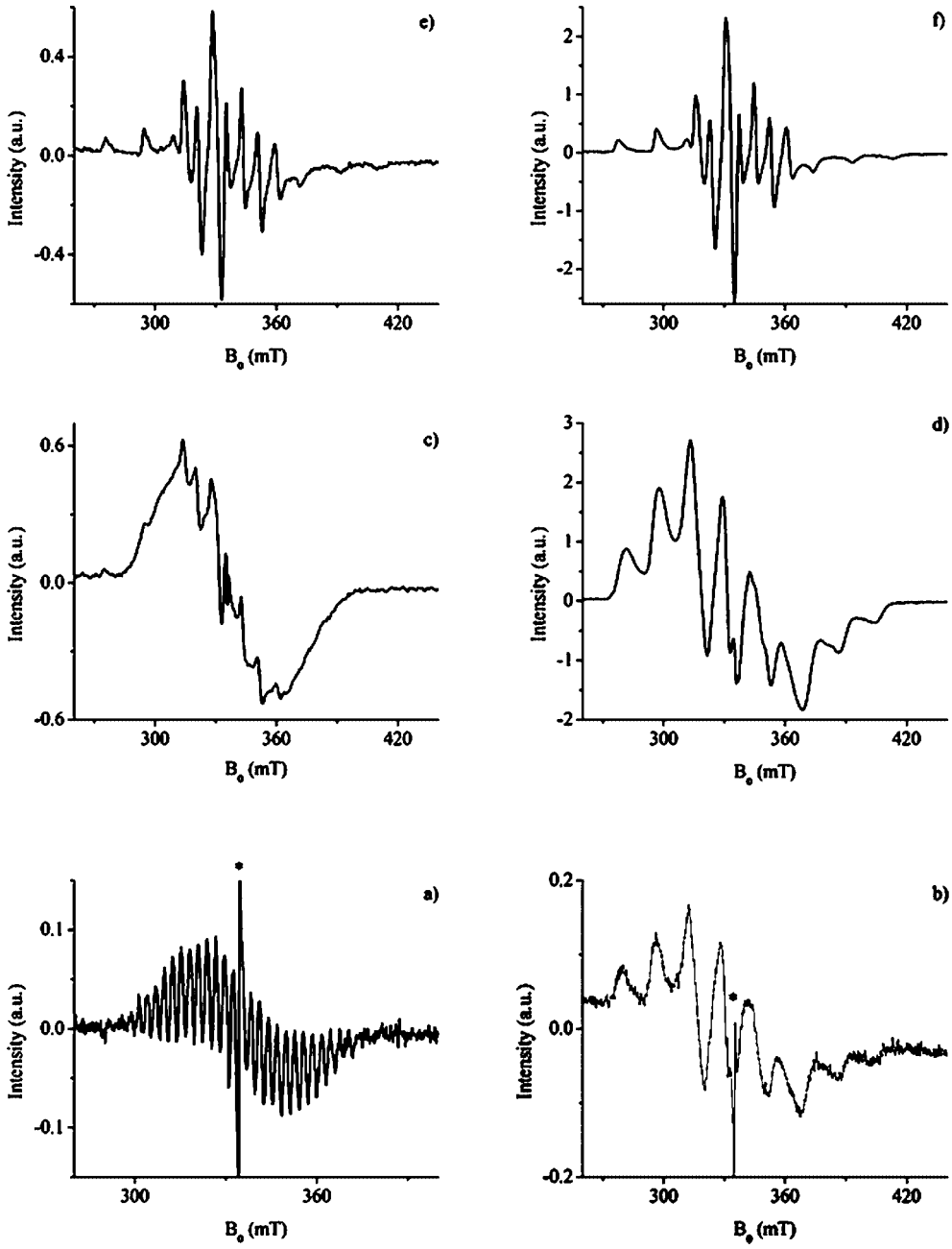

Figure 8. ESR spectra of $[(V_2O_3)_2(PhPO_3)_4 \subset F]^{2-}$ a) CH_3CN solution at 293 K; b) CH_3CN solution at 77 K; c) in contact with Al_2O_3; d) in contact with Al_2O_3 at 77 K; e) after washing of (c) with CH_3CN at 293 K; f) after washing of (c) with CH_3CN at 77 K. *: reference ($MgO:Cr^{3+}$ g = 1.9796).

well-resolved hyperfine multiplet consisting of 29 lines and A_{iso} = 28.6 G.

On the Localization/Delocalization of Spin Density in the Cage with S = 1/2

Comparison Between Experiment and Theory

The simulation[16] of the spectra obtained for the solution of $VO(acac)_2$ in CH_3CN at 293 K yields the following coupling constants: A_0 = 105. Because the quantum-chemical calculations refer to "free" molecules, the influence of polar or nonpolar solvents on the paramagnetic species in the experiments must be taken into account. The literature offers for $VO(acac)_2$ several values for the isotropic coupling constant in the range of 100 G.[13,14] Based on these values one can estimate a solvent-depending interval of ± 5 G for the isotropic coupling constant. Keeping in mind the general difficulties of the calculation of spin densities, there is an acceptable correspondence to the calculated value of 85 G (Table 5).

Inspecting the hyperfine coupling pattern of the solution of the cage S = 1/2 in CH_3CN at 293 K (Figure 8, a) the value of A_o = 28.6 G reflects the delocalization of the spin

density in the cage because this A value must be lower than ca. 100 G for a localization on one ^{51}V centre by factor of 1/4. But it must be taken into account that there is a negative spin density at the O atoms and small ones at the P atoms. Therefore, the experimental spectrum is governed by the splitting of the ^{51}V. Note that a splitting by the O atom is negligible because the natural abundance of the ^{17}O isotope is very small.

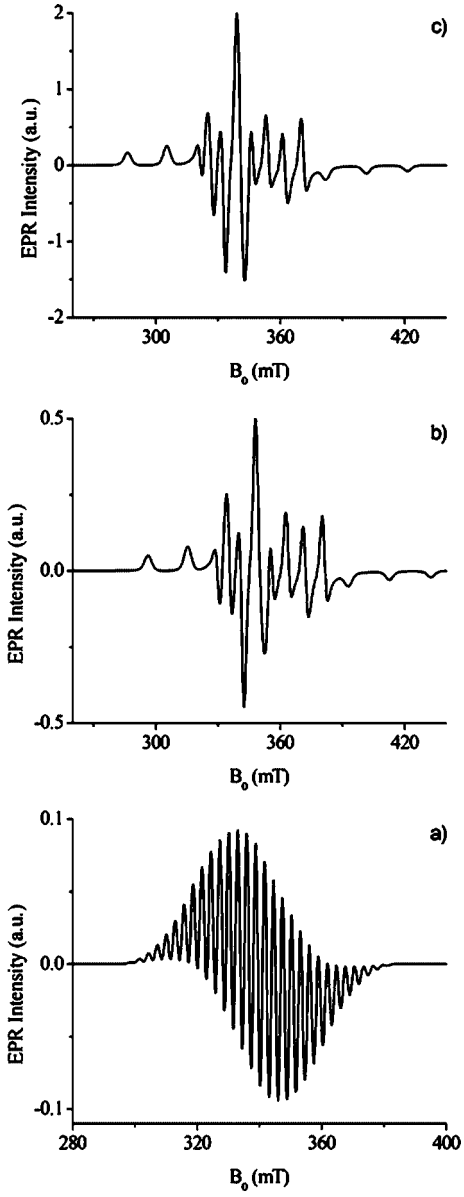

Figure 9. Simulated ESR spectra of $[(V_2O_3)_2(PhPO_3)_4\subset F]^{2-}$ a) CH_3CN solution at 293 K (g_{iso} = 1.964, A_{iso} = 28.6 G); b) in contact with Al_2O_3 and washing with CH_3CN at 293 K ($g_{\|}$ = 1.935, $A_{\|}$ = 195 G, $g_{\perp}$ = 1.986, $A_{\perp}$ = 72 G); c) in contact with Al_2O_3 and washing with CH_3CN at 77 K ($g_{\|}$ = 1.934, $A_{\|}$ = 69.6 G, $g_{\perp}$ = 1.982, $A_{\perp}$ = 192.8 G).Under structural aspects ESR investigation can be performed successfully if the hyperfine structure is only less disturbed by magnetic dipole–dipole and exchange interactions. This is best realized by the use of diamagnetically diluted systems, e.g. diluted solution or diluted single complexes respectively. The latter ones bear in principle the highest content of information but there are some experimental difficulties to prepare homogeneously diluted diamagnetic solids. For the title compound it was therefore easier to make use of the advantage of the solubility of $[Ph_3PCH_2CH_3][(V_2O_3)_2(PhPO_3)_4\subset F]$ in organic solvents.

Upon cooling, the ESR spectrum became gradually broad and no coalescence temperature could be distinct even below the freezing point of CH_3CN (230 K). The broad and unresolved line may due to the presence of different delocalization states i.e. 29, 21, and/or 15 lines (caused by the coupling with 4, 3 or 2 ^{51}V nuclei) which give the envelope of the hyperfine structure. The broad line was only found in the temperature range between the localized and fully delocalized states. However, the ESR of frozen solution (77 K) exhibits an 8 lines pattern (Figure 8, b) with a large degree of line broadening due to the anisotropy caused by the localization of the unpaired electron at one ^{51}V nucleus. The broad lines may indicate either that the hopping of the unpaired electron is still taking place to a small extend even at 77 K or that the electron becomes trapped on one vanadium atom with a partial spin density delocalization to other vanadium atoms in the cage (either through V–O–V and/or V–O–P–O–V). This for sure will give rise to more hyperfine lines which will contribute to the envelope. It is noteworthy that the spectral change between fluid and frozen solution is reversible which indicates that the cage compound retains its structure at these temperatures. A selection of simulated ESR spectra is given in Figure 9 together with the corresponding comments.

Simple Model Representation for the Delocalization of Spin Density in the Reduced Cage (S = 1/2)

At low temperatures "packing effects" are of influence on the cage geometry and electron distribution resulting in anisotropic ESR spectra exhibiting an eight-line pattern. This implies the localization of spin density at one ^{51}V nucleus. The result corresponds to that of the quantum-chemical calculations forcing the cage to C_s symmetry (Table 5). This configuration of the cage is represented by an energetically minimum at the potential surface which also leads to an essential localization of the spin density. The C_s symmetry of the cage could be also deduced from the results of XRD. The XRD could be performed on the cage system with S = 0 as well as with S = 1/2. The last one bears a high concentration of unpaired electrons in the solid sample which leads to an additional effect of spin-density delocalization. The spin exchange between the cages yields a single exchange narrowed ESR line which gives no direct information about the delocalization in the individual cages of the magnetically undiluted sample.

Rising the temperature of the frozen solution of the cage in the S = 1/2 state, the bond lengths and angles tend to fluctuate around temperature dependent (equilibrium) mean values. These mean values correspond to higher symmetries like C_{2v} or D_{2d} (see for example Table 5). In other words: driven by the thermal fluctuations these cage configurations of higher symmetry will be generated with a certain probability. The action of thermal energy induces a shift of the geometrical mean values and the bond lengths (Table 3) will be larger. It should be noted, that such states

of the cage must not represent minima at the potential surface. As a consequence of the admixture of such states at higher temperature (taking into account the actual solvent properties like dielectric constant, viscosity, polarity, etc.) a progressive delocalization of spin density appears in the cages. If the fluctuating D_{2d} symmetry reaches a large statistical weight, the delocalization is nearly complete. This is possible, because the fluctuations of the cage geometry are followed directly by fluctuations of the spin density.

Based on a rather classical aspect the process of spin density delocalization can be regarded as a "hopping process" of the unpaired electron inside the cage with $S = 1/2$. By this hopping, transition states can be reached in the time average which are in formal correspondence to the states obtained by the quantum chemical calculations using C_{2v} and D_{2d} symmetries.

The patterns of the ESR spectra of the mixed-valence system $[(V_2O_3)_2(PhPO_3)_4 \subset F]^{2-}$ measured in solution at room temperature are governed at least by three processes:

i) The hopping of the unpaired electron between the ^{51}V atoms present in the cage.

ii) The tumbling rate of the cage: the cage possess no spherical symmetry (maximal D_{2d}) even at fast hopping rate[20] a tumbling rate of ca. 10^{10} s^{-1} appears to be necessary to produce an isotropic and therefore optimal resolved ESR spectrum. This is approximately the case for the solution of the cage in the doublet state in acetonitrile ($\eta CH_3CN = 0.345$ mPas) (Figure 8, a) at 293 K.

iii) Fluctuation of the cage geometry likewise induced by thermal energy of the environment. But these fluctuations are limited by the template central F^- ion which tends to preserve the cage geometry.

In solution of higher viscosity, e.g. DMSO (η = 2.473 mPas), see also part c of Figure 6, spectral resolution of the ESR spectra will be achieved at higher temperature (e.g. 80 °C) where the tumbling of the cage is fast enough to resolve the 29-line spectrum [i.e. the coupling of the unpaired electron with 4 approximately equivalent ^{51}V nuclei ($I = 7/2$)].

At room temperature (Figure 8, a), the hopping is fast enough for the X-band ESR to detect the coupling with 4 equivalent ^{51}V nuclei. The rest anisotropy of the cage (D_{2d} symmetry or lower) prevents at lower tumbling rates a high spectral resolution because the individual hyperfine lines are too broad with respect to the values of the hyperfine constant of 28.5 G.

Obviously, the hopping rate at low-temperatures is much slower (e.g. $\approx 10^8$ s^{-1}). Therefore the frozen solution of the cage exhibits at 77 K an eight line spectrum (Figure 8, b) with evidences the localization of the unpaired electron at one ^{51}V nuclei. The broad lines result from less effective hopping at 77 K, producing additional but small hyperfine splitting.

Rising the temperature (up to ≈ 150 K) the eight-line spectrum with the relatively broad lines is more or less preserved. Above ca. 150 K the hopping process will be more effective, contributing more and more to the delocalization of the unpaired electrons and the eight-line spectrum is transformed to the envelope of the 29 line spectrum. The envelope results, because at this temperature there is no real tumbling which could average out the rest of the anisotropic hyperfine coupling. Increasing the temperature even more, up to the fluid system at 293 K, the combined effect of fast hopping and fast tumbling makes the spectral resolution as displayed in Figure 8 (a) possible.

The X-ray Structure

As shown in Figure 10 the structure of [Ag(1-methylimidazole)$_2$]$_2$[$(V_2O_3)_2(PhPO_3)_4 \subset F$] is constructed from the anionic cage fragment $[(V_2O_3)_2(PhPO_3)_4 \subset F]^{2-}$ which is already described in literature[3,4] and from two cationic [Ag(1-methylimidazole)$_2$] fragments. In each cationic frag-

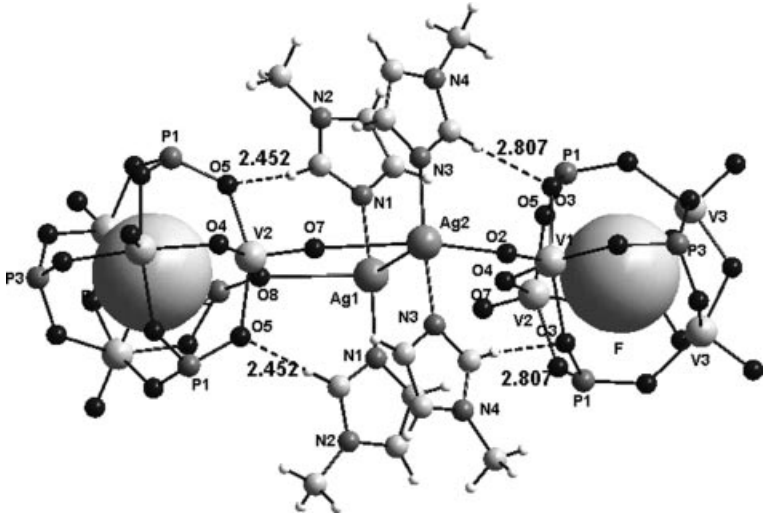

Figure 10. X-ray structure of part of 1D-chain compound [Ag(1-methylimidazole)$_2$]$_2$[$(V_2O_3)_2(PhPO_3)_4 \subset F$] showing the fluoride anion (with van der Waals radii) in the centre of the cage, hydrogen bonds between Ag(1-methylimidazole)$_2$ fragments and the O atoms of the cage and the Ag–Ag bond. Phenyl rings of the cage fragments were omitted for clarity.

ment, the Ag ion is coordinated by two nitrogen atoms of different 1-methylimidazole groups to make a nearly linear bond angles between N(1)–Ag(1)–N(1) (171.45°) and N(3)–Ag(2)–N(3) (173.04°). The Ag(1)–N(1) and Ag(2)–N(3) distances are 2.060 and 2.118 Å, respectively. The cationic parts are connected together through π-π stacking interactions between the methylimidazole moieties and through Ag(1)–Ag(2) bond (3.091 Å) which is shorter than the van der Waals contact distance (3.40 Å)[21] and slightly larger than Ag–Ag metallic bond (2.89 Å).[22]

The methylimidazole groups which are connected to the Ag(2) are laying in one plane while the 1-methylimidazole groups which are connected to the Ag(1) are lying in different planes (the angle between the methylimidazole planes is 24.046°). The cationic and anionic fragments are holding together through Ag–O bonds and through intermolecular hydrogen bonds to make 1D chain running along *x* axis. The Ag(2) ion is bonded to two cages through the vanadyl oxygen atoms, namely through the O(2) of one cage and through O(7) of another [Ag(2)–O(2) 2.659 Å, Ag(2)–O(7) 2.701 Å], which means that the cage acts as a ligand toward Ag^+ ions to create a 1D chain. Also, the cage is bonded to Ag(1) through O(8) [Ag(1)–O(8) 2.834 Å]. There are week intermolecular hydrogen bonds between the methylimidazole groups and oxygen atoms of the cage [H(19) with O(5) and H(23) with O(3)] and between hydrogen atom H(10) on the phosphonate phenyl group with Ag(2) [Ag(2)–H(10) 2.746 Å].

For Crystal data and structure refinement for [Ag(1-methylimidazole)$_2$]$_2$[$(V_2O_3)_2(PhPO_3)_4$⊂F] see Table 6. Selected bond lengths and angles are collected in Tables 7 and 8, respectively.

Table 6. Crystal data and structure refinement for [Ag(1-methylimidazole)$_2$]$_2$[$(V_2O_3)_2(PhPO_3)_4$⊂F].

Empirical formula	$C_{40}H_{44}Ag_2FN_8O_{18}P_4V_4$
Formula weight	1487.21
Temperature	180(2) K
Wavelength	0.71073 Å
Crystal system, space group	orthorhombic, *Pnma*
Unit cell dimensions	a = 16.775(2) Å, α = 90°
	b = 17.543(3) Å, β = 90°
	c = 18.248(3) Å, γ = 90°
V	5369.9(13) Å^3
Z, calculated density	4, 1.840 Mg/m^3
Absorption coefficient	1.582 mm^{-1}
F(000)	2956
Crystal size	0.24 × 0.20 × 0.16 mm
Theta range for data collection	2.23–25.25°
Limiting indices	$-20 \le h \le 20$,
	$-21 \le k \le 21$,
	$-21 \le l \le 21$
Reflections collected/unique	46121/5027 [R(int) = 0.0767]
Completeness to θ = 25.25	99.8%
Max. / min. transmission	0.7859 / 0.7026
Refinement method	full-matrix least squares on F^2
Goodness-of-fit on F^2	1.010
Final R indices [$I > 2\sigma(I)$]	$R1$ = 0.0385, $wR2$ = 0.0928
R indices (all data)	$R1$ = 0.0610, $wR2$ = 0.1035
Largest diff. peak and hole	0.719 and –1.279 e·A^{-3}

Table 7. Selected bond lenghts.

Atom 1	Atom 2	Distance [Å]
Ag1	Ag2	3.0910(8)
Ag1	N1	2.0600(53)
Ag2	N3	2.1178(35)
V1	O2	1.5869(35)
V1	O4	1.9153(37)
V1	O1	2.0024(38)
V1	O3	2.0165(30)
V1	O3	2.0165(30)
V1	F	2.4160(33)
V2	O7	1.5972(38)
V2	O4	1.7223(35)
V2	O5	1.9739(33)
V2	O5	1.9739(33)
V2	O8	2.0285(35)
V2	F	2.5372(31)
V3	O11	1.5807(34)
V3	O10	1.7983(20)
V3	O6	1.9083(32)
V3	O9	1.9323(30)
V3	O12	1.9367(28)
V3	F	2.4366(25)

Table 8. Selected bond angles.

Atom 1	Atom 2	Atom 3	Angle [°]
N1	Ag1	N1	172.94(21)
N3	Ag2	N3	175.08(13)
O2	V1	O4	103.70(17)
O2	V1	O1	96.59(17)
O2	V1	O3	101.76(8)
O2	V1	O3	101.76(8)
O2	V1	F	176.75(15)
O7	V2	O4	105.37(22)
O7	V2	O5	104.14(8)
O7	V2	O5	104.14(8)
O7	V2	O8	97.45(20)
O7	V2	F	175.25(16)
O11	V3	O10	100.63(14)
O11	V3	O6	98.90(15)
O11	V3	O12	100.94(15)
O11	V3	O9	101.75(15)

Conclusions

For all symmetries examined in this paper it has been shown that the doublet structures are more stable than the singlet ones. The geometries of the doublet structures depend essentially on the SOMO of the additional electron. From a purely empirical point of view without referring to quantum-mechanical calculations there is no definite statement about the residence of the additional electron possible. The hybrid DFT method, at least in the B3LYP version, is able to differentiate between delocalization and localization in mixed-valence vanadium organophosphonates. It should be noted that the amount of Hartree–Fock exchange[23,24] of the DFT functional is of special influence on the values calculated for the spin density. 20% of Hartree–Fock exchange seems to be a good choice for the calculation of delocalized spin densities. Generally, it could be stated that the tendency of delocalization of spin density rises with lowering of the amount of Hartree–Fock exchange. Reduc-

ing the Hartree–Fock exchange to 15% the localization of the additional electron was not realized (calculated by self-defined B3LYP functional in the frame of GAUSSIAN 03).

Comparison of the experimental and calculated hyperfine coupling constants (for doublet structure with D_{2d} symmetry) shows good agreement: ca. 28.6 and 27.5 G. Obviously, the stronger tendency of delocalization of spin density yields a better agreement between the results of the theoretical calculations and the experimental ones.

Lowering of the temperature down to 77 K causes localization of spin density which is announced by the eight line ESR spectrum resulting mainly from the interaction of the unpaired electron with one ^{51}V nucleus. At least two reasons can be quoted for this behaviour: (i) states generated in freezing process deform the cage via specific interaction and can end up in C_s symmetry; (ii) assuming the process of hopping for the spin-density delocalization, a lowering of the temperature diminished the rate (or the efficiency of the hopping of the unpaired electron) and the localization of spin density is favoured.

Further support for the localization results from the comparison of the spectrum with that of $VO(acac)_2$. This molecule is anisotropic (suffering from an axial perturbation) but the symmetrical cage cannot be deformed in such a way. Furthermore, one has to assume that some electron hopping occurs even at 77 K takes place in a restricted manner. This is of influence on the actual spectral pattern characterized by line widths and intensities, but they are able to change the averaged localization of spin density to a small extent.

It can be stated that the hyperfine coupling constant for the localized spin density (A_{iso} = 113 G) in the cages is in acceptable corresponds to the value calculated for the cage in C_s symmetry (85.3 G). No further discrete effects of the spin density localization (e.g. splitting from two or three ^{51}V nuclei) could be observed by ESR in the temperature range between 77 and 293 K. Therefore different probabilities should result to find the unpaired electron on 4, 3, 2, or 1 ^{51}V atom of the cage. The superposition of these probabilities yield a broad ESR line which represent the envelope of the hyperfine patterns resulting from splitting by 4, 3, 2, and 1 ^{51}V nucleus. Lowering of the temperature starting from 293 K to the range of ca. 200 K and below more and more increases the probability to find the unpaired electron at one ^{51}V nucleus.

Experimental Section

The synthesis of the cage compounds was carried out by a new route of synthesis using KF as a source of the fluoride anion.[5] All chemicals were of analytical grade.

X-ray: Data collection was carried out on an IPDS diffractometer (Stoe & Cie) at 180 K using graphite-monochromated Mo-K_α radiation and a cryostream cooler (Oxford Cryosystems). The data set was collected in steps of $\Delta\phi$ = 1.1° up to 198°. The measured intensities were corrected for background, Lorentz polarization, absorption and crystal decay effects. The structure was solved[25] and refined[26] with the SHELX 97 program.

ESR Spectroscopy: ESR spectra (X-band) were recorded using the spectrometer ERS 300 (ZWG/Magnettech., Berlin-Adlershof, Germany). The spectra were simulated using the programs Simfonia.[16] The temperature control unit E-257/WL-257 (Varian, USA) was applied for the variation of the temperature of the samples inside the cavity. Because of the lower limit of the temperature range was of interest ($T \geq 77$ K) which bears some difficulties with respect to the stability, a simple alternative to the gas-flow apparatus E-257 was used: a Dewar flask was filled with liquid nitrogen to cool the sample down to 77 K. Afterwards the liquid nitrogen was removed and the Dewar flask was closed. The temperature was raised with a flat exponential curve caused by the transport of the heat from the environment into the sample. The temperature was monitored using a thermocouple positioned inside the sample. In the same time, the ESR spectra were measured continually in a time interval of small temperature changes.

The following experiments were performed to transform the cage into the doublet state (S = 1/2) as well as to change the spatial distribution of the spin density inclusive the possible changes of the cage geometry:

i) By reaction of the cage compound $Ph_3PCH_2CH_3[(V_2O_3)_2(PhPO_3)_4F]$ with $(n\text{Bu})_4NI$ in CH_3CN one electron was transferred to the cage and the system persisted in the doublet state (S = 1/2). Then ESR spectra were measured at 293 and 77 K in a capillary tube (inner diameter, 1 mm).

ii) The paramagnetic solution (i) was treated with Al_2O_3 (Aldrich), then the solvent was removed and the ESR spectra of the solid (adsorbents/adsorbate) were measured at 293 and 77 K.

iii) The solid part of (ii) was washed with CH_3CN, and then the ESR spectra were measured at 293 and 77 K of both the solid and the solution.

CCDC-640689 contains the supplementary crystallographic data for this paper. These data can be obtained free of charge from The Cambridge Crystallographic Data Centre via www.ccdc.cam.ac.uk/data_request/cif.

Acknowledgments

The Deutscher Akademischer Austausch Dienst (DAAD) is acknowledged for financial support of Jabor K. Jabor. Dr. W. Hermann and Dr. A. Zehl are kindly acknowledged for supporting parts of the experimental works. Furthermore we thank Th. Ritschel for supporting the calculations.

[1] M. Vasylyev, R. Neumann, *Chem. Mater.* **2006**, *18*, 2781–2783.
[2] W. J. Johnson, A. J. Jacobson, W. M. Butler, S. E. Rosenthal, J. F. Brody, J. T. Lewandowski, *J. Am. Chem. Soc.* **1989**, *111*, 381–383.
[3] Q. Chen, J. Zubieta, *J. Chem. Soc. Chem. Commun.* **1994**, 2663.
[4] D. Thorn, R. Harlow, N. Herron, *Inorg. Chem.* **1995**, *34*, 2629–2638.
[5] to be published.
[6] J. Salta, Q. Chen, Y.-D. Chang, J. Zubieta, *Angew. Chem. Int. Ed. Engl.* **1994**, *33*, 757.
[7] Y.-D. Chang, J. Salta, J. Zubieta, *Angew. Chem. Int. Ed. Engl.* **1994**, *33*, 325.
[8] Q. Chen, J. Zubieta, *J. Chem. Soc. Chem. Commun.* **1994**, 1635.
[9] M. Meisel, D. Wulff-Molder, in preparation.
[10] D. Becke, *J. Chem. Phys.* **1993**, *98*, 5648; C. Lee, W. Yang, R. G. Parr, *Phys. Rev. B* **1988**, *37*, 875.
[11] In general the 6-311 G* has been used with a small change of the number of polarisation functions for different atoms. For

the 6-311G basis set see: A. D. McLean, G. S. Chandler, *J. Chem. Phys.* **1980**, *72*, 5639.
[12] M. J. Frisch, G. W. Trucks, H. B. Schlegel, G. E. Scuseria, M. A. Robb, J. R. Cheeseman, J. A. Montgomery Jr, T. Vreven, K. N. Kudin, J. C. Burant, J. M. Millam, S. S. Iyengar, J. Tomasi, V. Barone, B. Mennucci, M. Cossi, G. Scalmani, N. Rega, G. A. Petersson, H. Nakatsuji, M. Hada, M. Ehara, K. Toyota, R. Fukuda, J. Hasegawa, M. Ishida, T. Nakajima, Y. Honda, O. Kitao, H. Nakai, M. Klene, X. Li, J. E. Knox, H. P. Hratchian, J. B. Cross, C. Adamo, J. Jaramillo, R. Gomperts, R. E. Stratmann, O. Yazyev, J. Austin, R. Cammi, C. Pomelli, J. W. Ochterski, P. Y. Ayala, K. Morokuma, G. A. Voth, P. Salvador, J. J. Dannenberg, V. G. Zakrzewski, S. Dapprich, A. D. Daniels, M. C. Strain, O. Farkas, D. K. Malick, A. D. Rabuck, K. Raghavachari, J. B. Foresman, J. V. Ortiz, Q. Cui, A. G. Baboul, S. Clifford, J. Cioslowski, B. B. Stefanov, G. Liu, A. Liashenko, P. Piskorz, Komaromi, R. L. Martin, D. J. Fox, T. Keith, M. A. Al-Laham, C. Y. Peng, A. Nanayakkara, M. Challacombe, P. M. W. Gill, B. Johnson, W. Chen, M. W. Wong, C. Gonzalez, J. A. Pople, *Gaussian 03*, Revision B.02, Gaussian, Inc., Pittsburgh PA, **2003**.
[13] C. M. Guzy, J. B. Raynor, M. C. R. Symons, *J. Chem. Soc. A* **1969**, 2791–2795.
[14] M. Baltes, P. Van Der Voort, B. M. Weckhuysen, R. Ramachandra Rao, G. Catana, R. A. Schoonheyd, E. F. Vansanta, *Phys. Chem. Chem. Phys.* **2000**, *2*, 2673–2680.
[15] D. Kivelson, *J. Chem. Phys.* **1960**, *33*, 1094–1106.
[16] *WIN-SimFonia*, Bruker.
[17] G. B. Karet, Z. Sun, D. D. Heinrich, J. K. McCusker, K. Folting, W. E. Streib, J. C. Huffman, D. N. Hendrickson, G. Christou, *Inorg. Chem.* **1996**, *35*, 6450–6460.
[18] J. Jabor, R. Stößer, Nguyen Huu Thong, B.Ziemer, M. Meisel, to be published.
[19] J. A. R. Van Veen, G. Jonkers, W. H. Hesselink, *J. Chem. Soc. Faraday Trans. 1* **1989**, *85*, 389–413.
[20] S. P. Harmalker, M. A. Leparulo, M. T. Pope, *J. Am. Chem. Soc.* **1983**, *105*, 4286–4292.
[21] A. Bondi, *J. Phys. Chem.* **1964**, *68*, 441–451.
[22] D. Venkataraman, Y. Du, S. R. Wilson, K. Hirsch, P. Zhang, J. S. Moore, *J. Chem. Educ.* **1997**, *74*, 915–918.
[23] E. Ruiz, J. Cirera, S. Alverez, *Coord. Chem. Rev.* **2005**, *249*, 2649.
[24] K. R. Asmis, G. Santambrogio, M. Brümmer, J. Sauer, *Angew. Chem.* **2005**, *117*, 3182.
[25] G. M. Sheldrick, *Acta Crystallogr., Sect. A* **1990**, *46*, 467–473, cited for SHELXS.
[26] G. M. Sheldrick, *SHELXL-97*, Program for Crystal Structure Refinement, University of Göttingen, Göttingen (Germany), **1997**.

Received: January 23, 2007
Published Online: June 18, 2007

